

Plastic 95-GHz rectangular waveguides by micro molding technologies[☆]

Firas Sammoura^{a,*}, Yu-Chuan Su^a, Ying Cai^b, Chen-Yu Chi^c,
Bala Elamaram^c, Liwei Lin^a, Jung-Chih Chiao^b

^a Department of Mechanical Engineering, University of California at Berkeley, Berkeley, 1709 Shattuck Avenue, Suite 210, CA 94720-1740, USA

^b Department of Electrical Engineering, University of Texas at Arlington, Arlington, TX 76019-0016, USA

^c Agilent Technologies, 1400 Fountain Grove Pky, San Rosa, CA 95403, USA

Received 1 March 2005; received in revised form 11 July 2005; accepted 13 July 2005

Available online 13 October 2005

Abstract

A plastic, 95-GHz rectangular waveguide with an integrated plastic flange has been successfully demonstrated using micro hot embossing and electroplating technologies. Two prototype devices with integrated flanges on both ends have been tested using an Agilent PNA 5250 network analyzer. The prototype with non-metallized flange shows return loss s_{11} and insertion loss s_{21} values of -21.5 and -1.09 dB at 108 GHz, respectively with signal transmission rate at 77.8%. The prototype with metallized flange has s_{11} and s_{21} values of -31.5 dB and -0.7 dB, respectively, at 92.5 GHz, with signal transmission rate at 85%. The time domain measurement showed that the system losses are mainly due to the discontinuity losses at the interfaces between the network analyzer adaptors and the waveguide input/output ports. These losses could be further minimized in future integrated systems. As such, this new class of plastic waveguides has potential applications in replacing the expensive and bulky/heavy metallic waveguides in current millimeter-wave systems.

© 2005 Elsevier B.V. All rights reserved.

Keywords: Rectangular waveguide; Millimeter-wave; Hot embossing; W-band; Molding

1. Introduction

Millimeter-wave sensor systems could provide various sensing functionalities for all-weather applications [1], such as automobile crash avoidance systems, airplane radars [2–4], astronomy, weather monitoring and soil/moisture sensing [5]. Metal rectangular waveguides are commonly employed for millimeter-wave systems because of their lower attenuation compared to microstrip or stripline structures [6]. Currently, rectangular waveguides are fabricated using conventional machining techniques in metal and later assembled/mounted to construct a complete millimeter-wave system. High frequency systems demand small feature sizes such that micromachining technologies are natural alternatives. Previously, Tai et al. have demonstrated a silicon-based rectangular waveguide using bulk micromachining processes of a $\langle 100 \rangle$ -silicon wafer

with an insertion loss of 0.04 dB/ λ for a frequency range of 75–110 GHz [7]. LeDuc et al. integrated a superconductor-insulator-superconductor (SIS) tunnel junctions mounted on a nitride membrane with a bulk micromachined rectangular waveguide fabricated using wet etching of a $\langle 100 \rangle$ -silicon wafer. The waveguide was tested for a frequency range of 170–260 GHz and a 0.8 dB per wavelength insertion loss was measured [8]. Davies et al. have fabricated a reduced-height, air filled, surface-micromachined W-band rectangular waveguide. The waveguide performance was poor due to height limitation and the measured insertion loss was 0.2 dB/ λ [9]. Katehi et al. demonstrated a diamond-shape waveguide in W-band using wet etching of a $\langle 100 \rangle$ -silicon wafer and the mismatch between the WR-10 ports of the network analyzer and the diamond waveguide caused an insertion loss of 0.135 dB/ λ [10].

This work presents a plastic, hot-embossed, W-Band waveguide. In contrast to the previous works, three distinctive achievements have been accomplished: (1) plastic waveguides using batch embossing technologies [11,12], (2) metallic coating and sealing by selective electroplating and bonding, and (3) integrating a precision hot-embossed flange using press fitting/instant glue bonding with subsequent planarization. We believe this new

[☆] A portion of this paper was presented at the 18th IEEE Micro Electro Mechanical Systems Conference, Miami, 30 January–3 February, 2005, pp. 167–170.

* Corresponding author. Tel.: +1 510 642 8983; fax: +1 510 642 6163.
E-mail address: firmas@me.berkeley.edu (F. Sammoura).

technology provides the feasibility of low-cost manufacturing and integration with other micro electromagnetic-wave components, such as antennas, transmission lines, and phase-shifters for integrated millimeter-wave systems.

2. Theory and fabrication process

The cut-off frequency of a hollow metallic, air-filled rectangular waveguide could be found as [13]:

$$f_{c,mn} = \frac{1}{2\sqrt{\mu_0\epsilon_0}} \sqrt{\left(\frac{m}{a}\right)^2 + \left(\frac{n}{b}\right)^2} \quad (1)$$

where $f_{c,mn}$ is the cutoff frequency, μ_0 is the permeability of free space, ϵ_0 is the permittivity of free space, a is the width of the waveguide, b is the height of the waveguide, and m, n are integer numbers for the propagating modes. The desired fundamental mode in a rectangular waveguide is the transverse electric TE_{10} mode ($m=1$ and $n=0$). It is desirable to have the operating frequency higher by 60% than the cut-off frequency of the mode and lower by 25% of the cut-on frequency of the next mode. For 95-GHz systems, the design conditions are:

$$1.6f_{c,10} = 95 \text{ GHz} \quad \text{and} \quad 0.8f_{c,01} = 95 \text{ GHz} \quad (2)$$

and the dimensions of a W-band waveguide become 2.54 mm × 1.27 mm. For conventional millimeter-wave systems, the fabrication process of a waveguide/flange is typically done by precision machining on a metallic block followed by brazing a metallic cover to enclose the waveguide.

In the proposed plastic molding process as illustrated in Fig. 1 [14], an aluminum mold insert is fabricated by traditional mechanical machining and is used to pattern a plastic substrate to form an open waveguide using hot embossing at 320 °F. A tolerance of ±0.015 mm is required on the rectangular ridge of the mold. The mold is designed to process a plastic substrate with thickness of 2.5 mm and length of 25.4 mm. The plastic replica is then detached and subsequently a layer of 200 Å/6000 Å Cr/Pt is sputtered as the seed layer for the following electroplating step. A second silicon substrate is sputtered with 500 Å/6000 Å

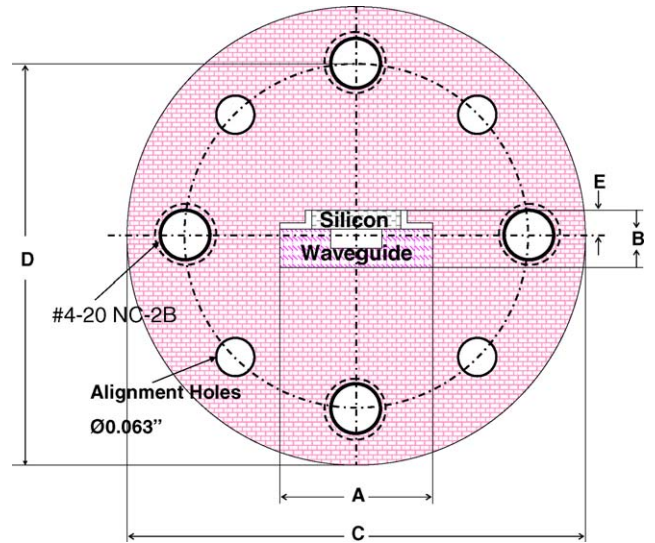


Fig. 2. A schematic diagram of the flange design showing how the waveguide with the silicon cap is press fitted and sealed. The dimensions A, B, C, D, and E are 10, 3, 19.1, 14.3, and 1.15 mm, respectively.

Cr/Pt combination and is clamped on top of the first substrate to cover the open waveguide. A flange adaptor is separately fabricated using the same hot embossing process in such a way that the open waveguide/silicon cover could be integrated with the adaptor to fit into the standard waveguide measurement instruments as shown in Fig. 2. Screw threads and pinholes are drilled at the precise locations with a tolerance of ±0.015 mm. The clamped combination of open waveguide/silicon cover is press fitted and glued using super glue (Loctite quicktite). The surfaces of the flange/press fitted waveguide are planarized using lapping with silicon carbide paper of very fine 600 grid mesh. The waveguide with integrated flange adaptor is then immersed into a gold electroplating solution (140 °F and 1000 rpm) to deposit an 8 μm-thick gold layer.

The selective electroplating process also metallurgically seals the waveguides [15]. Fig. 3 shows two SEM micrographs of the fabricated waveguide. From the preliminary observation, the

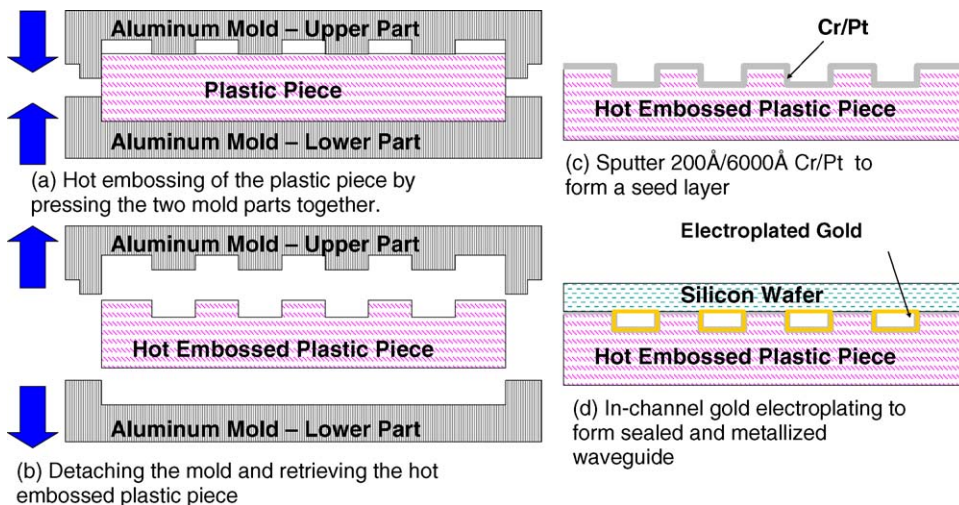


Fig. 1. Fabrication process of the waveguide.

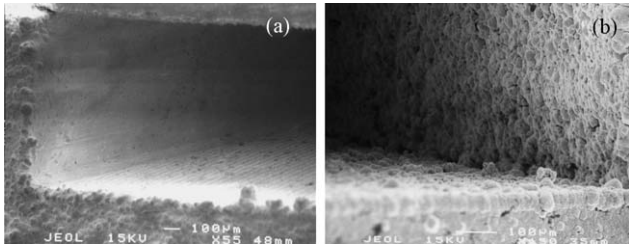


Fig. 3. SEM pictures of the waveguide. (a) The lower left corner of the waveguide and (b) close up view of the lower right corner showing good sealing between the 2 wafers.

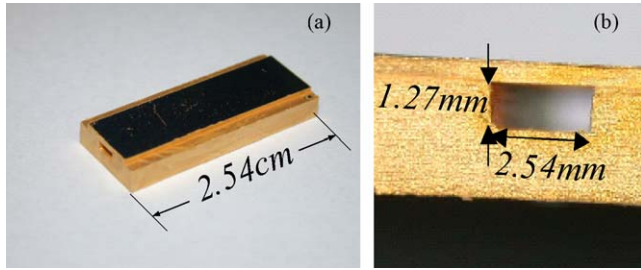


Fig. 4. (a) A photograph of the fabricated waveguide and (b) a close-up tilted view of the waveguide showing both the input and the output port.

metallic surface is smooth with a measured surface roughness using AFM [16] with RMS value of 1350 Å and the electroplated sealing is good with no observable leak. Fig. 4a is the photo of the fabricated waveguide that is 2.54 cm in length and Fig. 4b is the close-up tilted view of the waveguide showing both the input and the output ports. Fig. 5a is an optical photo of the prototype integrated with non-metallized flange adaptors at both ends and Fig. 5b is a close-up view of the flange showing the planner surface of the flange after the lapping process. Fig. 6 shows the photo of the prototype metallized flange sitting next to a conventional rectangular waveguide manufactured by Agilent Inc.

3. Results and discussion

The dimensions of the plastic 95-GHz rectangular waveguide were measured using a micrometer. The height and width of the waveguide are 1.295 mm and 2.515 mm, respectively. These

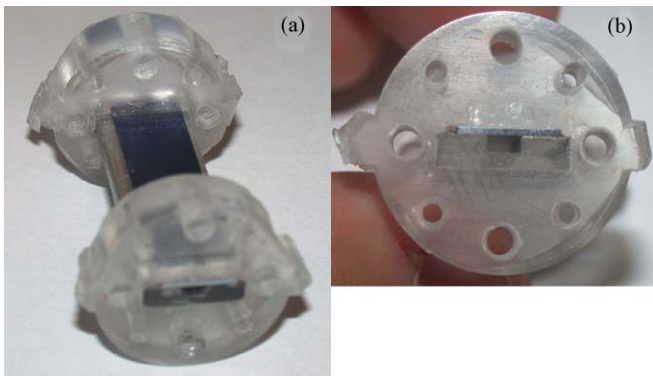


Fig. 5. Waveguide with non-metallized flange: (a) A photograph of the waveguide with integrated flange adaptors and no metallized flange walls; (b) a close up view at the flange adaptor.

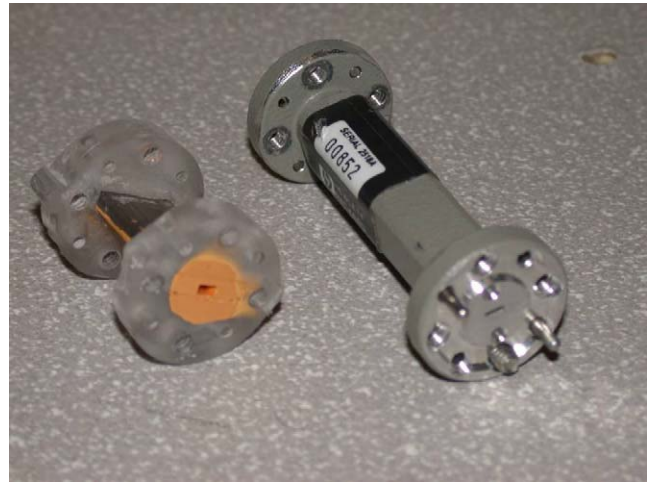


Fig. 6. Waveguide with metallized flange: (left) a microfabricated plastic 95 GHz waveguide with metallized flange; (right) a conventional metallic waveguide by Agilent Inc.

numbers fall within the acceptable tolerance of the guidelines of a standard metallic W-band waveguide that could allow for ± 0.03 mm variation in the waveguide cross-sectional dimensions [17]. The variations could be attributed to the shrinkage of the plastic as well as inaccuracies of the mold itself (the mold variation was +0.012 mm and -0.01 mm in ridge height and width, respectively).

The scattering parameters s_{11} (indicating return loss) and s_{21} (indicating transmission loss) of the waveguide are measured from 75 to 110 GHz using Agilent PNA 5250 network analyzer shown in Fig. 7a. Fig. 7b shows a close up view of the waveguide connected to a network analyzer. Fig. 8 is the measured frequency response for the waveguide without metallized flange. It is noted that the s_{11} was between -20 and -40 dB between 75 and 110 GHz while the typical metallic waveguide can have responses less than -40 dB. The resonant nulls are due to the interfaces at each end of the waveguide. The insertion loss parameter s_{21} varies between -1.79 dB at 75 GHz to -1.06 dB at 110 GHz. At 95 GHz, the insertion loss is -1.35 dB and the return loss is -20.7 dB. The guided wavelength of the propagating wave inside a hollow, air-filled rectangular waveguide is a function of frequency and could be calculated as follows [13]:

$$\lambda_g = \frac{2\pi}{\sqrt{\omega^2 \mu_0 \epsilon_0 - (\pi/a)^2}} \quad (3)$$

where λ_g is guided wavelength of the TE₁₀ mode, ω is the radian frequency in rad./s, μ_0 and ϵ_0 are the permeability and permittivity of free space, respectively, and a is the width of the waveguide. It is calculated that at 95 GHz, λ_g is 4.03 mm and a waveguide length of 25.4 mm corresponds to 6.3 wavelengths. Thus the insertion loss per wavelength at 95 GHz becomes 0.214 dB/ λ_g (0.531 dB/cm). This is larger than the nominal value of 0.026 ~ 0.028 dB/cm in a commercial WR-10 single-mode metallic waveguide without connectors.

The relatively poor performance of the waveguide comes from the interface contact losses between the waveguide and the measurement apparatus. The time domain measurement in

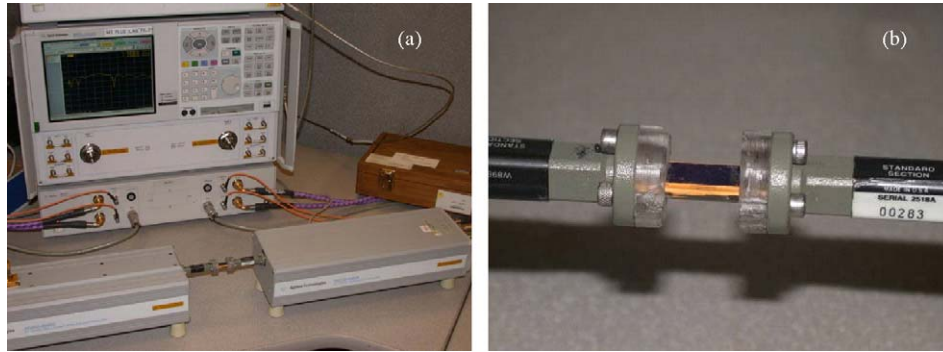


Fig. 7. Testing set-up. (a) Agilent PNA 5250 network analyser; (b) close up view of waveguide connected to a network analyser.

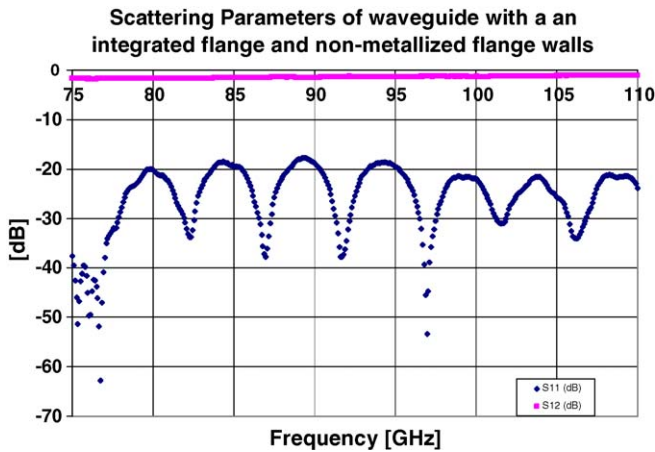


Fig. 8. Scattering parameters for the waveguide with non-metallized flange measured using Agilent network analyzer PNA 5250. At 95 GHz, the return loss parameter, s_{11} , is -20.7 dB and the insertion loss parameter, s_{21} , is -1.35 dB.

Fig. 9 verified this. The time domain plot of the return loss parameter s_{11} showing the major reflections are at the interfaces between the input/output port and the network analyzer adaptor. The peak at the point 1 shows the return loss at 0 s when the signal passes port 1, and the peak at point 3 shows the signal

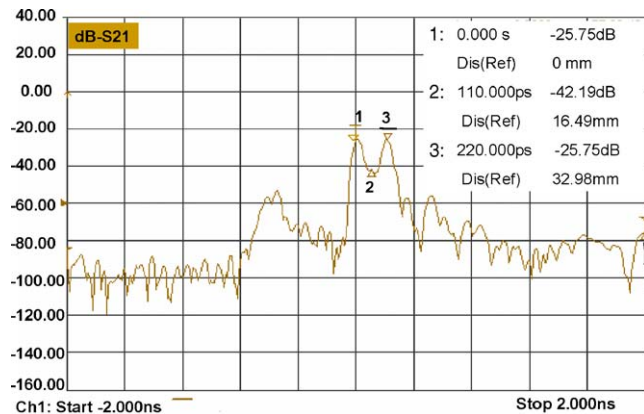


Fig. 9. A time domain log-scale plot of the return loss parameter, s_{11} , showing the major reflection losses are at the interfaces between the input/output ports and the network analyzer adaptor. The peak at point 1 shows the return loss at 0 s (port 1), and the peak at point 3 shows the return loss after 220 ps (port 2). The small reflection in between comes from the waveguide itself.

reflected after 220 ps back from port 2. The small reflection in between comes from the waveguide itself. It is worth mentioning that a full trip of the wave from port 1 to port 2 and back to port 1 takes 220 ps. The group velocity, v_g , of a propagating wave with a single carrier frequency inside a hollow rectangular waveguide could be calculated as [13]:

$$v_g = \frac{\sqrt{\omega^2 \mu_0 \epsilon_0 - (\pi/a)^2}}{\omega \mu_0 \epsilon_0} \quad (4)$$

The group velocity at 75 and 110 GHz is 1.85×10^8 and 2.53×10^8 m/s, respectively. The time required for a wave to make one trip from port 1 to port 2 of a waveguide of 25.4 mm in length varies from 100 ps at 110 GHz to 137 ps at 75 GHz. The 110 ps travel time measured from the network analyzers falls within this range. The difference between the theoretical and experimental data is due to the fact that in calculating the time domain data, the network analyzer uses *Inverse Fast Fourier Transform technique* (IFFT), which assumes a constant propagation constant within the 75–110 GHz frequency range.

Fig. 10 is a time domain plot of the transmission parameter s_{21} , showing that maximum transfer of energy occurs at point 2 after 110 ps, i.e. at the output interface. The loss is thus mainly concentrated at the input and output ports and is attributed to the small gap between the flange/waveguide connection the network analyzer adaptor due to the non-metallized flange surface.

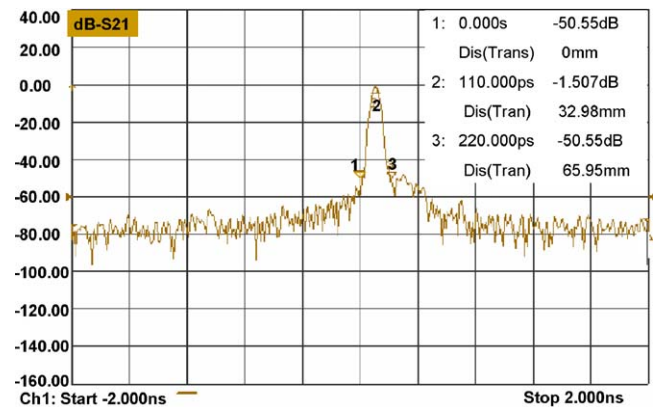


Fig. 10. A time domain log-scale plot of the insertion loss parameter, s_{21} , showing the maximum transfer of energy occurred at point 2 after 110 ps (when the wave arrives at port 2).

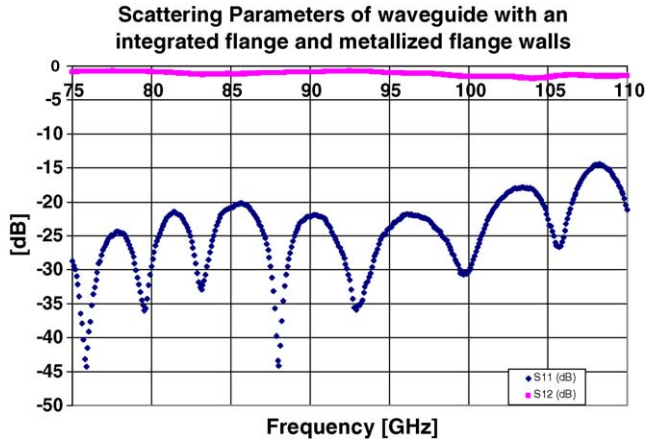


Fig. 11. Scattering parameters of the waveguide with metallized flange measured using Agilent network analyzer PNA5250. At 95 GHz, the return loss parameter, s_{11} , is -24.5 dB and the insertion loss parameter, s_{21} , is -0.96 dB. At 92.5 GHz, s_{11} is -31.5 dB and s_{21} is -0.7 dB (85% transmission).

This issue can be resolved in an integrated system where all the connection interfaces are integrated and fabricated at the same time.

In order to reduce the interface contact losses between the waveguide and the measurement apparatus, the surface of the flanges in contact with the network analyzer adaptors was metallized. The scattering parameter results for the waveguide with metallized flanges are shown in Fig. 11. The best performance was measured at 92.5 GHz: the return loss s_{11} was -31.5 dB and the insertion loss s_{21} was -0.7 dB and the insertion loss per wavelength is 0.116 dB/ λ_g (0.276 dB/cm). At 95 GHz the s_{11} and the s_{21} values were -23.9 and -0.99 dB, respectively, and the insertion loss per wavelength is 0.157 dB/ λ_g (0.39 dB/cm).

For a reciprocal ($[S_{ij}] = [S_{ij}]^*$) and no loss network, one has [18]:

$$\sum_{k=1}^N s_{ki} s_{ki}^* = 1 \quad (5)$$

For a two-port network, Eq. (5) becomes:

$$|s_{11}|^2 + |s_{21}|^2 = 1 \quad (6)$$

Whenever the summation of transmission and return losses does not add up to the unity, there is dissipation within the system. The dissipation is mainly due to imperfectly reflecting walls. The attenuation factor α_c could be theoretically calculated as follows [18]:

$$\alpha_c = \frac{P_{\text{loss}}}{2P_{\text{total}}} = \frac{R_s}{a^3 b \beta \omega \eta \sqrt{\mu_0 \epsilon_0}} (2b\pi^2 + a^3 \omega^2 \mu_0 \epsilon_0) \left[\frac{Np}{m} \right] \quad (7)$$

where R_s is the sheet resistance of the waveguide surface, a and b are the width and height of the waveguide, respectively, β is the propagation constant, ω is the frequency, μ_0 and ϵ_0 are the permeability and permittivity of free space, respectively. The measured conductivity of the electroplated film using a four point probe was 1.5×10^6 Ω m. Fig. 12 compares the attenuation coefficient, α_c , versus frequency for both experimental and theoretical data. The experimental attenuation coefficient is obtained with the interface losses since we cannot separate them

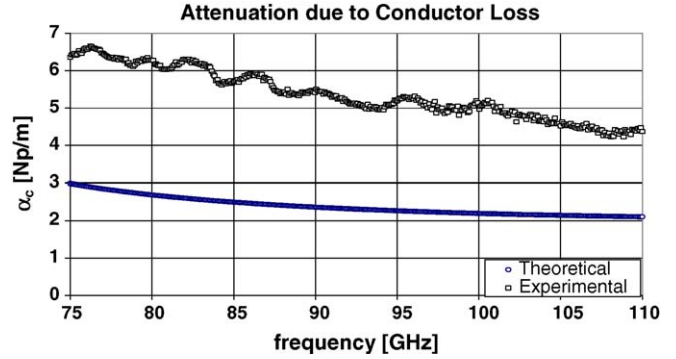


Fig. 12. Experimental and theoretical attenuation due to conductor loss vs. frequency.

form our measurement. The two plots follow the same trend of decreasing attenuation coefficient versus frequency. The difference between theoretical and experimental values is due to other unaccounted losses such as dielectric losses as well as signal leakage/radiation at the input/output interfaces.

4. Conclusion

Plastic 95-GHz rectangular waveguides have been demonstrated. The waveguide has been batch fabricated using inexpensive hot embossing and electroplating techniques. Two prototype waveguides with integrated flanges on both sides have been tested walls using an Agilent PNA 5250 network analyzer. The measured scattering parameters s_{11} (return loss) and s_{21} (transmission loss) from 75 to 110 GHz for the first prototype without a metallized flange show minimum insertion loss of -1.06 dB at 109.6 GHz, which corresponded to 0.129 dB/ λ_g . The performance was further improved by fixing the discontinuity between the waveguide itself and the network analyzer cable adaptors by metallizing the flange surface. The measured scattering parameters s_{11} and s_{21} for the second prototype with a metallized flange show improvement as minimum insertion loss of -0.7 dB at 92.5 GHz, which corresponded to 0.116 dB/ λ_g . The attenuation coefficient due to conductor losses was also calculated and compared to theoretical predictions. An attenuation of 5.2 Np/m was measured at 95 GHz compared to 2.3 Np/m predicted from theory. The discrepancy is again due to the measurement interface. It is envisioned that this new class of waveguides could facilitate the integration of other millimeter-wave components such as antennas, filters [19], and phase shifters toward an integrated system.

Acknowledgements

This project is supported in part by NSF grant DMI-0428884 and these devices were fabricated in the UC-Berkeley Microfabrication Laboratory and the Mechanical Engineering Machine Shop. The authors would like to thank Mr. Ron Wilson for taking the SEM pictures and Mr. John Morton at the Mechanical Engineering Department at UC-Berkeley for fabricating the molds.

References

- [1] H. Akimoto, Atmospheric measurement of chemical species using spectroscopic technique, in: 10th Anniversary. Advanced Technologies in Instrumentation and Measurement Technology Conference, IMTC/94, vol. 1, May, 1994, p. 7.
- [2] B. Macqueen, J. Mcqueen, Intelligent Transportation Systems Architecture, Artech House, Boston, MA, 1999.
- [3] Y. Zhou, Vehicle Location and Navigation Systems, Artech House, Boston, MA, 1997.
- [4] H.P. Groll, J. Detlefsen, History of automotive anti-collision radar and final experimental results of a mm-wave car radar developed on the Technical University of Munich, in: Proceedings of 1996 CIE International Conference for Radar, 1996, pp. 13–17.
- [5] J.B. Mead, A.L. Pazmany, S.M. Sekelsky, R.E. McIntosh, Millimeter-wave radars for remotely sensing clouds and precipitation, in: Proceedings of the IEEE, vol. 82, no. 12, December, 1994, pp. 1891–1906.
- [6] F. Gardiol, Microstrip Circuits, Wiley, 1994, pp. 13.
- [7] W.R. McGrath, C. Walker, M. Yap, Y.C. Tai, J. Silicon Micromachined Waveguides for Millimeter-Wave and Submillimeter-Wave Frequencies, Microwave Guided Wave Lett. vol. 3 (no. 3) (1999) 61–63.
- [8] J.A. Wright, S. Tacic-Lucic, Y.C. Tai, W.R. McGrath, B. Bumble, H. LeDuc, Integrated Silicon Micromachined Waveguide Circuits For Submillimeter Wave Applications, in: Symposium Proceedings: Sixth International Symposium on Space Tetrahertz Technology, March, Pasadena, CA, 1995, pp. 387–396.
- [9] J.W. Digby, C.E. McIntosh, G.M. Parkhurst, S.R. Davies, Fabrication and Characterization of Micromachined Rectangular Components for Use at Millimeter and Tetrahertz Frequencies, IEEE Trans. Microwave Theory Tech. vol. 48 (no. 8) (2000) 1293–1302.
- [10] J.P. Becker, J.R. East, L.P.B. Katehi, Performance of silicon micromachined waveguide at W-band, Electronics Lett. vol. 38 (no. 13) (2002).
- [11] X.-J. Shen, Li-Wei Pan, Liwei Lin, Microplastic embossing process: experimental and theoretical characterizations, Sens. Actuators A 97–98 (2002) 428–433.
- [12] L. Liwei, Y.T. Cheng, C.-J. Chiu, Comparative study of hot embossed microstructures fabricated by laboratory and commercial environments, Microsystem Technol. J. 4 (no. 3) (1998) 113–116.
- [13] Kraus/Fleisch, Electromagnetics with Application (McGraw-Hill, 1999), pp. 456–468.
- [14] F. Sammoura, Y.-C. Su, Y. Cai, C.-Y. Chi, B. Elamaram, L. Liwei, J.-C. Chiao, Microfabricated plastic 95-GHz rectangular waveguide, in: Proceedings of 18th IEEE Micro Electro Mechanical Systems Conference, 30 January–3 February, Miami, Florida, 2005, pp. 167–170.
- [15] Li-Wei Pan, Liwei Lin, Batch Transfer of LIGA Microstructures by Selective Electroplating and Bonding, IEEE/ASME J. Microelectromechanical Syst. 10 (2001) 25–32.
- [16] Digital Instruments Nanoscope 3100 atomic force microscope.
- [17] http://we.home.agilent.com/upload/cmc_upload/All/Agilent.Waveguide_Overview1.pdf.
- [18] D.M. Pozar, Microwave Engineering, Addison-Weseley, 1990, p. 226.
- [19] F. Sammoura, Y. Cai, C.-Y. Chi, T. Hirano, L. Liwei, J.-C. Chiao, A micromachined W-band iris filter, in: The 13th International Conference on Solid-State Sensors, Actuators and Microsystems, 5–9 June, Seoul, Korea, 2005, pp. 1067–1070.